ACS NANO
Cite This: ACS Nano 2019, 13, 9965−9972
www.acsnano.org

ARTICLE

Fiber-Integrated Reversibly Wavelength-Tunable Nanowire Laser Based on Nanocavity Mode Coupling

Ming-Hua Zhuge,[†] Zongyin Yang,[‡] Jianpei Zhang,[§] Yazhi Zheng,[†] Qinghai Song,[∥] Chenlei Pang,[†] Xu Liu,[†] Salman Ullah,[†] Caofeng Pan,[⊥] Nagarajan Raghavan,[#] Xing-Hong Zhang,[⊗] Haifeng Li,[†] Yaoguang Ma,*[,†] Qing Yang,*[,†,▽] and Tawfique Hasan[‡]

[†]State Key Laboratory of Modern Optical Instrumentation, College of Optical Science and Engineering, Zhejiang University, Hangzhou 310027, China

[‡]Cambridge Graphene Centre, University of Cambridge, Cambridge CB3 0FA, United Kingdom

[§]Sichuan Zhongguang Lightning Protection Technologies Co., Ltd., Chengdu 611731, China

[∥]Integrated Nanoscience Lab, Department of Electrical and Information Engineering, Harbin Institute of Technology, Shenzhen 518055, China

[⊥]Beijing Institute of Nanoenergy and Nanosystems, Chinese Academy of Sciences, National Center for Nanoscience and Technology (NCNST), Beijing 100083, China

[#]Engineering Product Development (EPD) Pillar, Singapore University of Technology and Design, 8 Somapah Road, Singapore 487372, Singapore

[⊗]MOE Key Laboratory of Macromolecular Synthesis and Functionalization, Department of Polymer Science and Engineering, Zhejiang University, Hangzhou 310027, China

[▽]Collaborative Innovation Center of Extreme Optics, Shanxi University, Taiyuan 030006, China

Supporting Information

ABSTRACT: **As an ideal miniaturized light source, wavelength-tunable nanolasers capable of emitting a wide spectrum stimulate intense interests for on-chip optoelectronics, optical communications, and spectroscopy. However, realization of such devices remains a major challenge because of extreme difficulties in achieving continuously reversibly tunable gain media and high quality (Q)-factor resonators on the nanoscale simultaneously. Here, exploiting single bandgap-graded CdSSe NWs and a Fabry−Pérot/whispering gallery mode (FP/WGM) coupling cavity, a free-standing fiber-integrated reversibly wavelength-tunable nanolaser covering a 42 nm wide spectrum at room temperature with high stability and reproducibility is demonstrated. In addition, a 1.13 nm tuning spectral resolution is realized. The substrate-free device design enables integration in optical fiber communications and information. With reversible and wide, continuous tunability of emission color and precise control per step, our work demonstrates a general approach to nanocavity coupling affording high Q-factors, enabling an ideal miniaturized module for a broad range of applications in optics and optoelectronics, with optical fiber integration.**

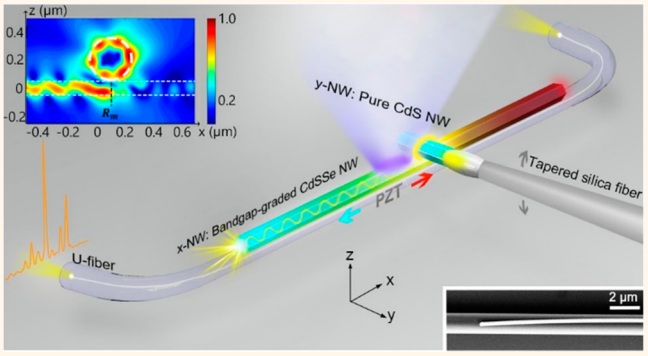

KEYWORDS: *nanolaser, wavelength reversibly tuning, nanocavity coupling, individual nanostructure, fiber-integrated*

Micro-/nanoscale lasers have great potential applications and are highly desired in on-chip optical communications and data processing.[1−8] Continuous and reversible wavelength tuning of nanolasers is indispensable for their practical applications in various fields,[9−20] such as wavelength-division multiplexing,[21,22] biomedical sensing,[23,24] and spectroscopy.[25] Numerous efforts have been made to achieve wavelength-variable nanolasers

Received: July 4, 2019
Accepted: August 9, 2019
Published: August 9, 2019

DOI: 10.1021/acsnano.9b05110
ACS Nano 2019, 13, 9965−9972

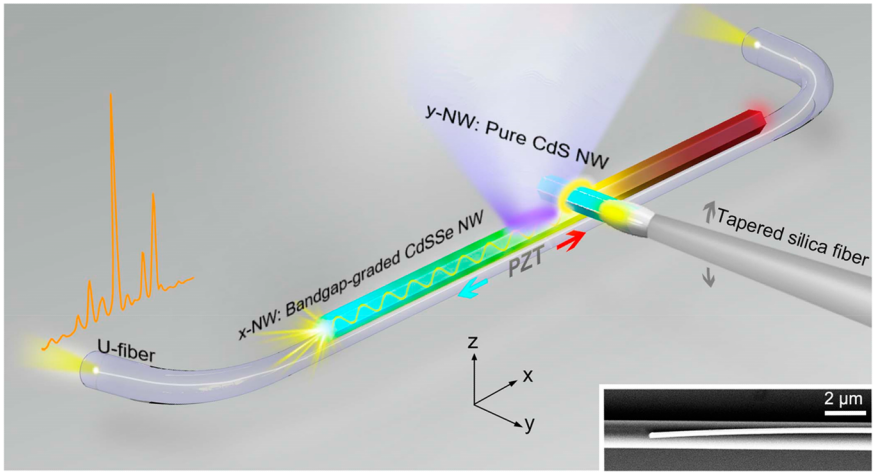

Figure 1. Schematic diagram of the fiber-integrated device and pump-collection process. Inset: SEM characterization of bandgap-graded CdSSe NW adhered to the U-fiber twist section. The diameters of the bandgap-graded CdSSe NW and U-fiber twist section are 313 nm and 1.33 μm, respectively.

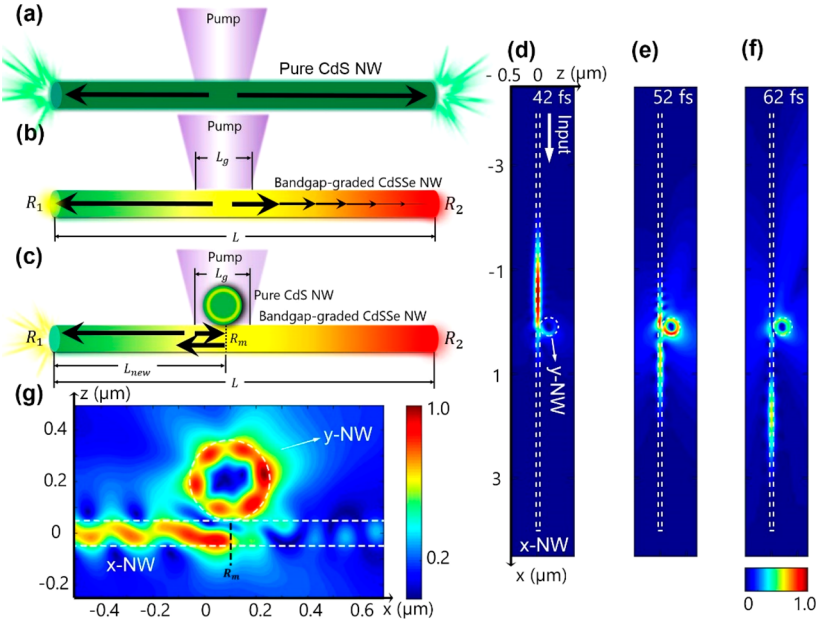

Figure 2. (a) Schematic diagram of FP cavity on a pure CdS NW based on end-facet reflection. The Q-factor is low due to the strong diffraction effect on the nanoscale. (b) Schematic diagram of FP cavity on a single bandgap-graded NW. In this case of being pumped at this particular position, no lasing occurs due to strong absorption. (c) Schematic diagram of an FP-WGM coupling cavity. One pure CdS NW is vertically placed on the bandgap-graded NW shown in (b). The newly formed resonator of length L_{new} has combined FP and WGM cavities and the coupling point serves as a resonator facet with high reflectivity (R_m). In both (b) and (c), the lengths of NW and pumped area are L and L_g, respectively, and $R_{1,2}$ are the reflectivities of the wide-bandgap and narrow-bandgap end-facets, respectively. (d–f), Transient light transmission process of a 3.3 fs duration pulse propagating and coupling in the FP-WGM hybrid structure, short-time snapshots at 42, 52, and 62 fs, respectively. (d) Short pulse propagates from the x-NW top surface and arrives at the coupling point; coupling begins here. (e) Most of the energy is coupled into y-NW, while a small portion of the light continues along the original path. (f) Photons stored in the WGM have a longer lifetime because of the high Q-factor of the WGM cavity served by the radial wall of y-NW. (g) The simulated result for steady-state solution of pulse transmission.

utilizing different methods, *e.g.*, absorption−emission−absorption effect by precisely cutting NWs step-by-step,[16,26] plasmon polariton-enhanced Burstein−Moss effect[27] by changing the dielectric layer thickness, varying the temperature,[28,29] and controlled synthesis of multiquantum-well core/shell NW heterostructures.[30] However, continuously and reversibly wavelength-tunable, wide-spectra nanolasers on single nanostructures at room temperature are yet to be realized.

The main challenge is how to exploit wide-spectra gain media and achieve a reversibly tuning high Q-factor resonator simultaneously. Almost all wide-spectra-tuning nanolasers on individual nanostructures are based on one-dimensional (1D) nanostructures, owing to their multifunctional use as gain media, resonance cavity, and waveguide and tuning ability.[31−37] Nanotechnology developments over the last two decades have afforded two routes for designing the resonator cavity geometry and utilizing spectral profile of gain media on

DOI: 10.1021/acsnano.9b05110
ACS Nano 2019, 13, 9965−9972

1D nanostructures. However, serious issues remain in both approaches. The most common uses of cavities on 1D nanostructures are based on end-facet reflection (see Figure 2a).[13,16,38] The Q-factor of this kind of cavity—one of the key factors of lasers—is low due to the strong diffraction effect of the end facets on the nanoscale. The Q-factor of a 120 nm diameter 1D nanostructure is calculated as ~200.[39] Another cavity design utilizes the Sagnac effect and ring coupling.[40−42] Although this improves the cavity Q-factor, only <10 nm-tuning range or several discrete-wavelength lasers can be obtained due to lack of utilization wide spectra gain media.

Combining spatial composition-graded gain media with cavity design is an emerging concept. Beyond the facile bandgap-graded nanomaterial growth, it is critically essential to explore a cavity structure in which the lasing of all emission colors can be allowed to emit with minimal material absorption while overcoming strong diffraction effect. Here, we propose a nanocavity coupling method to achieve wide-wavelength reversibly tunable nanolasers utilizing individual bandgap-graded CdSSe NWs. By establishing a vertical contact between a bandgap-graded CdSSe NW and a pure CdS NW (CdSSe-CdS-NWs), an FP-WGM coupling cavity is formed, with CdSSe as the gain medium. Our scheme yields a fiber-integrated wavelength-tunable lasing source with a 42 nm reversible spectral range, high stability and reproducibility. Our proposed method has the potential to support an extension of the spectral range beyond 100 nm with further material synthesis optimization.

RESULTS AND DISCUSSION

In our design shown in Figure 1, bandgap-graded CdSSe NWs were synthesized *via* a source-moving chemical vapor deposition (CVD) method.[43] The NW composition was changed evenly and gradually from the CdS bandgap to CdSe bandgap. To fully utilize the emission colors, a new cavity was formed by creating movable resonator facets at the vertical contact point of the CdSSe-CdS-NWs. In this configuration, the bandgap-graded CdSSe NW (*x*-NW) was adhered to a U-shaped microfiber (U-fiber), while the pure CdS NW (*y*-NW) (see Figure S3 of the Supporting Information) was adhered to a tapered silica fiber for ease of manipulation. A 3-dimentional PZT stage was utilized to finely control the positions of U-fiber and tapered fiber (see the Methods). In this fiber-integrated system, spectra collected by the U-fiber were sent to the optical spectrometer directly to confirm the stability of device. Compared with a structure over a planar substrate usually accompanied by strong van der Waals force, the fiber-integrated design yielded a substrate-free and suspended structure, which enabled device miniaturization along with smooth operation and convenient spectral measurement (see Figures S1 and S2 of the Supporting Information).

Unlike pure semiconductor NWs such as CdS NWs[33] in Figure 2a, the lasing wavelength of a bandgap-graded NW is strictly defined by the photoluminescence (PL) center wavelength of the narrow-bandgap end due to the asymmetric bandgap absorption of the bandgap-graded NWs.[13,44] As shown in Figure 2b, assuming that the length of NW is L while L_g is where the gain occurs, for the case without coupling, the following threshold condition is obtained (see Figure S4 of the Supporting Information)[45]

$$\Gamma g_{th} L_g = \alpha_{ab} L + \frac{1}{2} \ln \frac{1}{R_1 R_2} \quad (1)$$

where Γ represents the confinement factor, g_{th} denotes the threshold of the material gain coefficient, α_{ab} represents the material absorption coefficient, and the $R_{1,2}$ terms represent the reflectivities of the wide-bandgap and narrow-bandgap end-facets, respectively. The bandgap-graded NW's PL changes gradually with varying pump section. When a particular position on the bandgap-graded NW (excluding the narrow-bandgap end) is pumped, the threshold condition cannot be satisfied because of the strong asymmetrical material absorption in the narrow-bandgap section[13,44] (*i.e.*, $\alpha_{ab} L \gg \Gamma g_{th} L_g$). Therefore, a wavelength-tunable NW laser cannot be achieved by simply changing the pump section or increasing the pump density.[13,46]

In previous reports, defects were introduced to enable light scattering to form new cavities on single bandgap-graded CdSSe nanoribbons (see Figure S4d of the Supporting Information).[47] However, since the cavities were fixed by the defect positions, continuous tuning was impossible. In addition, due to the low scattering efficiency and strong diffraction effect of the scattering point, the Q-factors were very low, yielding high thresholds.

Our proposed hybrid structure design featuring the FP-WGM coupling cavity facilitates a higher Q-factor wavelength-tunable NW laser, where FP and WGM cavities coupling was designed to introduce a movable and tunable higher-Q-factor resonator. In the new resonator with a length L_{new} shown in Figure 2c, the emitting light propagates between the wide-bandgap end and coupling point. In this section, the emitting light energy is lower than the corresponding bandgap energy of the materials. Hence, the absorption for this case, α'_{ab}, is much smaller than α_{ab}. As shown in Figure 2d−f, the field intensities at different moments (42, 52, and 62 fs, respectively) indicate the light transmission process in such a hybrid structure. Some light transmitted from the top surface of *x*-NW couples into *y*-NW, traveling around the radial wall of the *y*-NW to form the WGM. FP mode in *x*-NW is mostly stored between the pulse source and coupling point, causing the latter to serve as a resonator facet with high reflectivity (R_m) (see Figure 2g). The WGM cavity has far superior photon storage than the FP cavity, which appears as owning higher Q-factors as we discuss later (see Figures S5 and S6 of the Supporting Information). According to experimental results (see Figures S7 of the Supporting Information), the threshold in our designed coupling condition is 50% reduced compared with the initial NW lasers, which indicates $R_m > R_2$. For an FP-WGM coupling cavity, a higher Q-factor is obtained than that for an FP cavity based on the end-facet reflection or contact point scattering. Therefore, eq 1 can be rewritten as

$$L_g \Gamma g_{th} = \alpha'_{ab} L_{new} + \frac{1}{2} \ln \frac{1}{R_1 R_m} \quad (2)$$

As $\alpha'_{ab} \ll \alpha_{ab}$, $L_{new} < L$ and $R_m > R_2$, all of which profit from the FP-WGM coupling cavity, the threshold reduces considerably and the lasing threshold can be reached more easily. A reversibly wavelength-tunable NW laser may thus be realized based on the FP-WGM coupling-cavity hybrid structure. Note that three different materials were considered as resonator facets in this study; however, CdS NWs exhibited the best performance in lowering the threshold (see Table S1 of the Supporting Information).

To confirm the laser oscillation in the FP-WGM nanocavity, the lasing spectra of another bandgap-graded CdSSe NW and two different coupling cavities based on the NW are presented

DOI: 10.1021/acsnano.9b05110
ACS Nano 2019, 13, 9965−9972

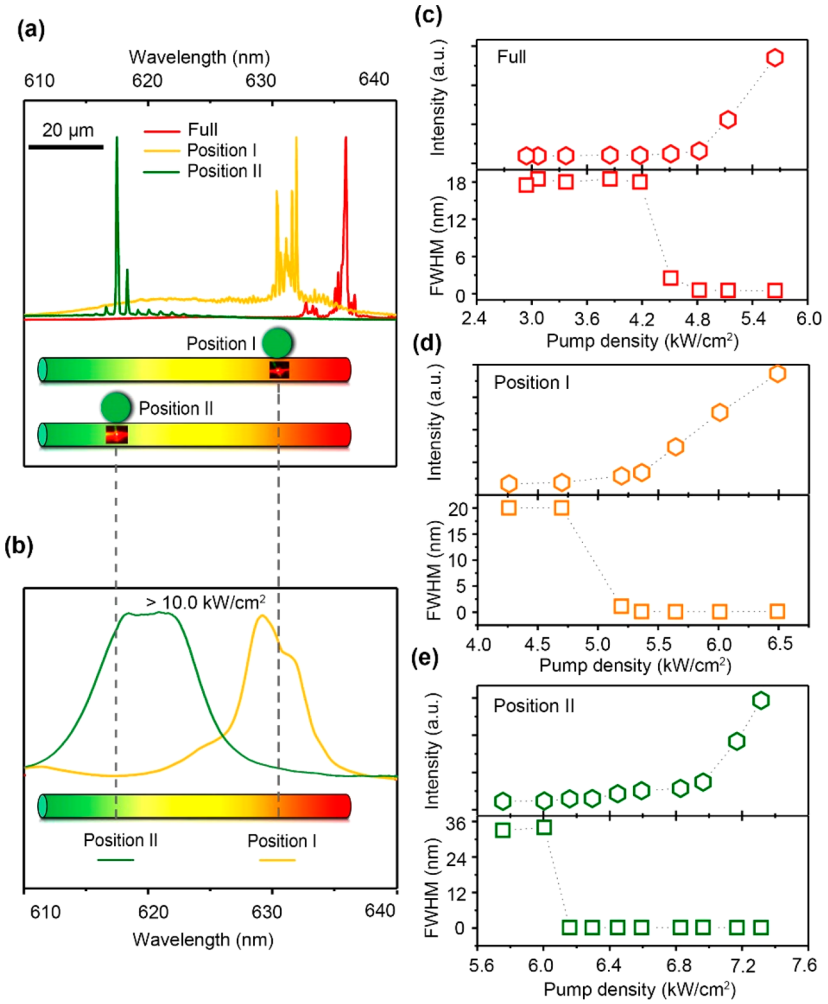

Figure 3. (a) Lasing spectra and real-color microscope images of the narrow-bandgap end and different coupling points in a same bandgap-graded CdSSe NW. The local images of colorful spots attached on the below bandgap-graded NW model were cut off from the coresponding CCD images. (b) PL spectra of position I and position II without coupling. The pump density was above 10 kW/cm^2. (c–e) The corresponding threshold curves (upper) and fwhm of the spectra (below) for the same full CdSSe NW, CdSSe NW with coupling cavity at position I, and CdSSe NW with coupling cavity at position II, respectively.

in Figure 3a. The corresponding threshold curves and fwhm are recorded in Figure 3c–e. The threshold of full NW laser with the center lasing wavelength of 636 nm was ~4.8 kW/cm^2. Without coupling, the PL spectra failed to convert to lasing in positions I and II owing to the ultrahigh thresholds (see Figure 3b). After introducing effective coupling points, the corresponding thresholds decreased dramatically, contributing to lasing at 631 and 618 nm, respectively. Above the threshold power density, the sharp peaks with <0.50 nm fwhm were developed.

We note that for an FP-WGM coupling cavity, when the pump section was fixed, the localized PL was converted to lasing at the wavelength defined by the coupling point, which was introduced in the narrower-bandgap side of the pump section (see Figure S8 of the Supporting Information). In addition, when the coupling point was fixed, the lasing wavelength depended on the pump sections: when the narrow-bandgap section was pumped, the lasing wavelength was defined by the narrow-bandgap end; when the wide-bandgap section was pumped, the lasing wavelength was defined by the bandgap of the coupling position (see Figure S9 of the Supporting Information). It is concluded that an effective coupling point and correct selection of the pump section are necessary for reversible lasing wavelength tuning. Here, WGM acting as a reflective facet has small volume in nanoscale, so that the FSR is also given by an approximate expression:[48] FSR = $\lambda^2/2n_gL$, where L is the length of resonator and n_g is the effective gourp index of refraction at wavelength λ. Before coupling, the initial FSR is 0.76 nm (see Figure S9b of the Supporting Information), while it becomes 1.77 nm after coupling (see Figure S9a of the Supporting Information). The n_g is calculated to be 4.98 and 5.38, respectively, which are consistent with the reported values.[13,42] Transverse modes are observed both in FP and FP-WGM cavities (as shown in Figure S10 in the Supporting Information), which indicates that the polarization of propagating lasing emission along the x-NW under FP-WGM coupling keeps the same as that in the initial FP cavity.

On the other hand, as for the lateral WGM cavity size which is in nanoscale, the coupling is effective. As shown in Figure S11 of the Supporting Information, after coupling, the fwhm has decreased considerably from 0.11 to 0.06 nm while the FSR has increased from 1.28 to 2.37 nm. Moreover, through simulation, the effect resulting from the gap distance between

DOI: 10.1021/acsnano.9b05110
ACS Nano 2019, 13, 9965–9972

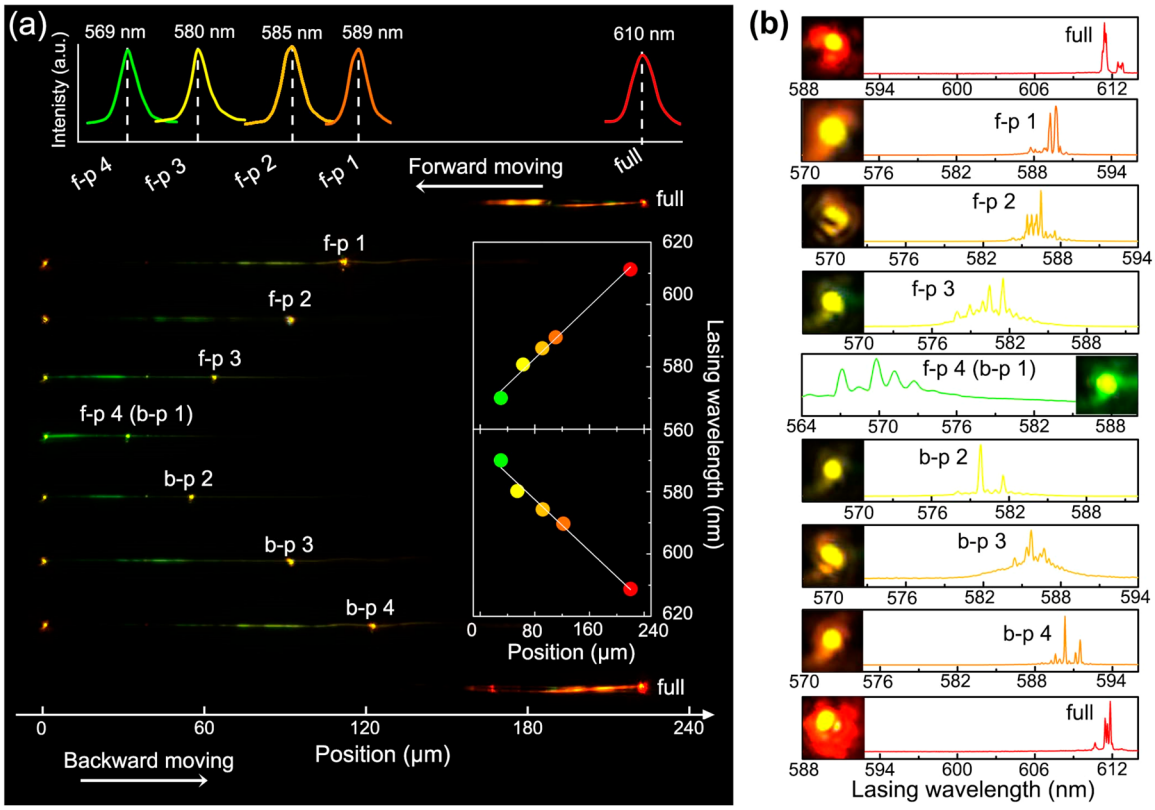

Figure 4. Reversible wavelength tuning over wide range for the bandgap-graded CdSSe NW identical to that in the inset of Figure 1. (a) Real-color microscope images of NW laser after introduction of FP-WGM coupling cavities with four forward (f-p 1−4) and backward points (b-p 1−4), where b-p 1 is identical to f-p 4. Inset (upper): Localized PL spectra at different coupling points in the same NW under low pump density by a 355 nm pulsed laser. Inset (right): Relationship between coupling point positions and lasing wavelengths. (b) Lasing spectra of the bandgap-graded CdSSe NW under reversible tuning. The colorful spots shown in each spectrum correspond to the real-color image of the end emission of the bandgap-graded CdSSe NW at pump density above the threshold shown in (a).

the two NWs is shown in Figure S12 of the Supporting Information. According to the simulation results, as the gap distance increases, the coupling efficiency is gradually enhanced up to the optimized (gap = 50 nm), and then goes down.[49,50] Due to strong van der Waals force between the two NWs, the distance of <100 nm is hard to control. Therefore, there was no gap between the two NWs in experiments.

Reversible wavelength tuning spanning more than 40 nm was achieved experimentally on the bandgap-graded CdSSe NW with 225 μm length and 313 nm diameter. The upper inset of Figure 4a presents the PL spectra of different positions on the same bandgap-graded CdSSe NW locally excited under low pump density by a 355 nm pulsed laser. The measured center wavelength of PL was from 569 to 610 nm. Four forward and four backward coupling points were successfully produced. The average distance between these contiguous points was ~30 μm. The center wavelengths gradually changed from 612 to 570 nm and then returned to 612 nm as the coupling point was moved back and forth. The linear relationship between the coupling positions and lasing wavelengths indicates that the wavelength variation was proportional to the moving distance (see Figure 4a, the right inset). This demonstrates the good control and reversibility of our experiment. From these real-color microscope images, the variable tendency of the coupling point colors could be judged. During forward movement, the color changed from red to green but became increasingly red for backward movement. The sharp line in the spectra indicates laser emission and tunability (see Figure 4b).

To further prove the stability and reproducibility of the wavelength tuning process, tuning of a bandgap-graded CdSSe NW with 125 μm length and 350 nm diameter for six cycles by alternating the coupling point between two positions (positions I and II) was examined (see Figures 5a). In the experiment, the average spacing between coupling positions I and II was approximately 40 μm and the coupling point was repeatedly alternated. In the six-cycle process, the lasing wavelengths changed between 608 (position I) and 601 nm (position II) with standard deviations of 0.50 and 0.19 nm, respectively, as shown in Figures 5b,c. For this representative switching, the average fluctuation was much smaller than the signal. The outstanding stability and reproducibility demonstrated by the data conclusively prove that our nanoscale fiber-integrated system can sufficiently achieve highly accurate reversible wavelength tuning of nanolaser.

Our method afforded not only wide-spectrum wavelength tuning, high accuracy, and reproducibility but also precise 1.13 nm resolution tuning (see Figure S13 of the Supporting Information). The wavelength varied in a 1.08 nm resolution when the coupling point was moved forward. For the reverse process in the backward direction, tuning with a 1.18 nm resolution was achieved, with a return to the same wavelengths and positions. Comparison of the two data sets confirms the high resolution and reliability of the wavelength tuning approach.

DOI: 10.1021/acsnano.9b05110
ACS Nano 2019, 13, 9965−9972

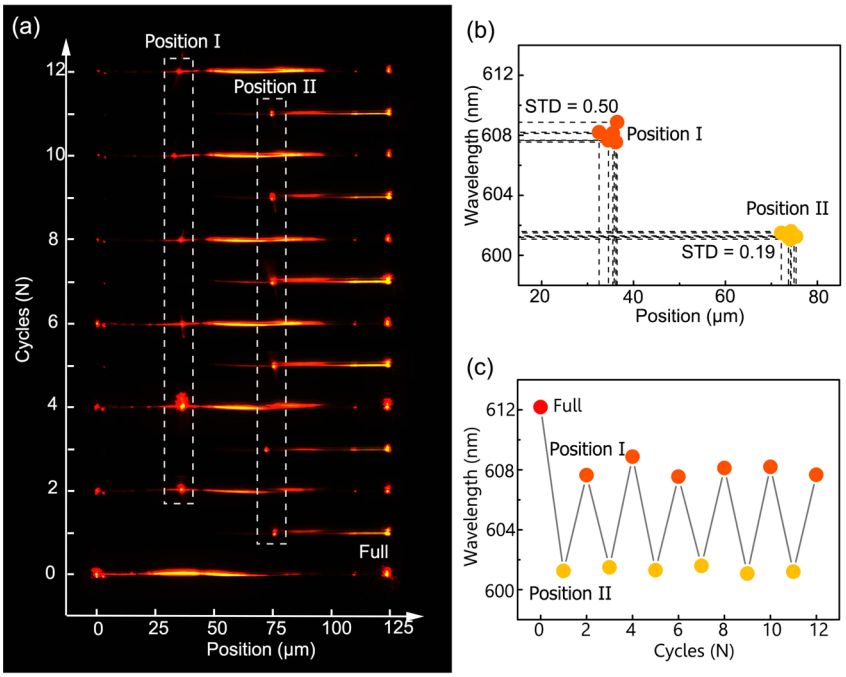

Figure 5. Stability and repeatability of reversibly wavelength-tunable NW laser. (a) Real-color microscope images of a bandgap-graded CdSSe NW with 125 μm length and 350 nm diameter. Six cycles of repeated switching between coupling points (positions I and II) were considered. (b) Corresponding lasing wavelengths of positions I and II fluctuate slightly with standard deviations of 0.50 and 0.19 nm, respectively. (c) Output lasing wavelengths with repeated switching of coupling points (positions I and II), showing stability and reproducibility of the lasing wavelengths.

CONCLUSIONS

In summary, utilizing the advantages of an FP-WGM coupling cavity, a room-temperature fiber-integrated reversibly wavelength-tunable nanolaser was demonstrated on a single bandgap-graded CdSSe NW with excellent accuracy, stability, wavelength-tuning repeatability, and high spectral resolution. This demonstration has several important implications. First, this achievement is a critical research step in fiber-integrated reversibly tunable nanolasing sources, and supports device miniaturization and integration in optical fiber communications. Second, as pumping and measurement can be performed through the fibers and the tuning process can be electrically modulated by the PZT stage, the fiber-integrated device can be used as a portable sensor or monitor suitable for operation in ambient atmosphere and at room temperature, further promoting semiconductor NW applications. Third, since the FP-WGM coupling cavity has an obvious advantage over the FP cavity, addition of multiple NWs onto a bandgap-graded NW could help realize single-NW-based multilasing wavelength emission. Our reversibly wavelength-tunable laser is expected to have wide and significant applications in next-generation integrated-field optics, sensing, and optical communications.

METHODS

Preparation of NWs and Samples. We synthesized bandgap-graded CdSSe and pure CdS NWs by using source-movable[43] and regular chemical vapor deposition[51] systems, respectively. After synthesis, the NWs were transferred to a substrate and pumped. Then good-quality NWs were picked up by a homemade silica fiber probe. Under an optical microscope (Zeiss AXIO Imager.A2m), the picked bandgap-graded CdSSe and pure CdS NWs were adhered to a U-fiber twist section and the tip of a tapered fiber, respectively. The U-fiber and tapered fiber were homemade by heating and stretching a section of a commercial optical fiber (Corning, SMF-28). To ensure the effectiveness of the coupling cavity, the bandgap-graded CdSSe and pure CdS NWs should be exactly above the U-fiber twist section and under the tip of the tapered fiber. In the proposed design, the U-fiber was fixed on a PZT stage (PI E-463.00) for precise 2D X-Y movement. The total displacement of PZT moving range is around 80 μm. The precision is measured as ~80 nm/step (see Figure S14 of the Supporting Information). The tapered fiber was fixed on the Z-dimensional stage moving in harmony with the U-fiber (see Figure S1), so that the pump section and coupling point varied simultaneously according to the bandgap-graded NW. This allowed the PL to vary gradually. With a steady pump beam, when the pure CdS NW touched the bandgap-graded CdSSe NW, the contact point naturally became an FP-WGM coupling point, acting as the new lasing-wavelength-defined point (see Figure S2a of the Supporting Information).

Sample Characterization. The structural characterization of the U-fiber twist section adhered to the bandgap-graded CdSSe NW was performed by scanning electron microscopy (SEM, Ultra55/ZEISS). After conducting experiments under the optical microscope, we carefully cut the U-fiber twist section with the entire bandgap-graded CdSSe NW and fixed these components on a silicon substrate for observation (see Figure S2b).

Optical Measurements. As shown in Figure S1, the bandgap-graded CdSSe NW was excited by a 355 nm pulsed laser obtained from a frequency-tripled Nd:YAG laser (10 kHz, 10 ns pulse width, MPL-N-355−500 mW), which was coupled directly to an optical microscope by a 50× objective. The objective focused the 355 nm pump beam with a diameter of ~20 μm. For stable and convenient spectral measurement, the spectrum was collected directly from the U-fiber and guided into a spectrometer (HORIBA Jobin Yvon iHR 550).

ASSOCIATED CONTENT

Supporting Information

The Supporting Information is available free of charge on the ACS Publications website at DOI: 10.1021/acsnano.9b05110.

DOI: 10.1021/acsnano.9b05110
ACS Nano 2019, 13, 9965−9972

Figures S1−S14: Experimental setup, SEM image of CdS NW, schematic diagrams of different strategies for cavity design; FDTD simulated results of light field distributions and Q-factors of FP/FP-WGM/FP-Scattering cavities; comparison of pure CdS NW laser thresholds before and after coupling; PL and lasing spectra analysis under different conditions; polarization analysis of one pure CdS NW before and after coupling; fwhm, FSR and lasing modes analysis of another pure CdS NW before and after coupling; FDTD simulated results of different gap distance between FP and WGM cavities; high spectral tuning resolution reversibly realized on a single bandgap-graded CdSSe NW; displacement of the fiber probe sticking with the coupling material *vs* PZT instrument reading; Table S1: Thresholds of CdS/CdSSe NWs after coupling with different coupled materials (PDF)

AUTHOR INFORMATION

Corresponding Authors

*E-mail: mayaoguang@zju.edu.cn.
*E-mail: qingyang@zju.edu.cn.

ORCID

Caofeng Pan: 0000-0001-6327-9692
Xing-Hong Zhang: 0000-0001-6543-0042
Qing Yang: 0000-0001-5324-4832

Notes

The authors declare no competing financial interest.

ACKNOWLEDGMENTS

We thank Xiaowei Liu, Pengfei Xu, Xuechu Xu, Mingwei Tang, and Zhong Wen for helpful discussions and Yingxin Xu and Ni Yao for help with the fabrication of U-fiber. This work is supported by the National Key Basic Research Program of China (No. 2015CB352003), the National Natural Science Foundation of China (Nos. 61822510, 61735017 and 51672245), the Zhejiang Provincial Natural Science of China (No. R17F050003), the Fundamental Research Funds for the Central Universities, the Program for Zhejiang Leading Team of S&T Innovation, the Cao Guangbiao Advanced Technology Program, and First-Class Universities and Academic Programs. T.H. and Q.Y. acknowledge funding support from the Royal Society through an international exchange scheme.

REFERENCES

(1) Kirchain, R.; Kimerling, L. A Roadmap for Nanophotonics. *Nat. Photonics* **2007**, *1*, 303−305.
(2) Jiang, X.; Yang, Q.; Vienne, G.; Li, Y.; Tong, L.; Zhang, J.; Hu, L. Demonstration of Microfiber Knot Laser. *Appl. Phys. Lett.* **2006**, *89*, 143513.
(3) Ma, J.; Xiao, L.; Gu, J.; Li, H.; Cheng, X.; He, G.; Jiang, X.; Xiao, M. Visible Kerr Comb Generation in a High-Q Silica Microdisk Resonator with a Large Wedge Angle. *Photonics Res.* **2019**, *7*, 573−578.
(4) Li, B.-B.; Clements, W. R.; Yu, X.-C.; Shi, K. B.; Gong, Q. H.; Xiao, Y.-F. Single Nanoparticle Detection Using Split-Mode Microcavity Raman Lasers. *Proc. Natl. Acad. Sci. U. S. A.* **2014**, *111*, 14657−14662.
(5) Ma, R.-M.; Oulton, R. F. Applications of Nanolasers. *Nat. Nanotechnol.* **2019**, *14*, 12−22.
(6) Wang, S.; Chen, H.-Z.; Ma, R.-M. High Performance Plasmonic Nanolasers with External Quantum Efficiency Exceeding 10%. *Nano Lett.* **2018**, *18*, 7942−7948.
(7) Wu, Z.; Chen, J.; Mi, Y.; Sui, X.; Zhang, S.; Du, W.; Wang, R.; Shi, J.; Wu, X.; Qiu, X.; Qin, Z.; Zhang, Q.; Liu, X. F. All-Inorganic $CsPbBr_3$ Nanowire Based Plasmonic Lasers. *Adv. Opt. Mater.* **2018**, *6*, 1800674.
(8) Liu, Z.; Shang, Q.; Li, C.; Zhao, L.; Gao, Y.; Li, Q.; Chen, J.; Zhang, S.; Liu, X. F.; Fu, Y.; Zhang, Q. Temperature-Dependent Photoluminescence and Lasing Properties of $CsPbBr_3$ Nanowires. *Appl. Phys. Lett.* **2019**, *114*, 101902.
(9) He, X.; Liu, P.; Zhang, H.; Liao, Q.; Yao, J.; Fu, H. Patterning Multicolored Microdisk Laser Arrays of Cesium Lead Halide Perovskite. *Adv. Mater.* **2017**, *29*, 1604510.
(10) Zhou, H.; Yuan, S.; Wang, X.; Xu, T.; Wang, X.; Li, H.; Zheng, W.; Fan, P.; Li, Y.; Sun, L.; Pan, A. Vapor Growth and Tunable Lasing of Band Gap Engineered Cesium Lead Halide Perovskite Micro/Nanorods with Triangular Cross Section. *ACS Nano* **2017**, *11*, 1189−1195.
(11) Zapf, M.; Röder, R.; Winkler, K.; Kaden, L.; Greil, J.; Wille, M.; Grundmann, M.; Schmidt-Grund, R.; Lugstein, A.; Ronning, C. Dynamical Tuning of Nanowire Lasing Spectra. *Nano Lett.* **2017**, *17*, 6637−6643.
(12) Ma, W.; Lu, J.; Yang, Z.; Peng, D.; Li, F.; Peng, Y.; Chen, Q.; Sun, J.; Xi, J.; Pan, C. Crystal-Orientation-Related Dynamic Tuning of the Lasing Spectra of CdS Nanobelts by Piezoelectric Polarization. *ACS Nano* **2019**, *13*, 5049−5057.
(13) Yang, Z. Y.; Wang, D. L.; Meng, C.; Wu, Z. M.; Wang, Y.; Ma, Y. G.; Dai, L.; Liu, X. W.; Hasan, T.; Liu, X.; Yang, Q. Broadly Defining Lasing Wavelengths in Single Bandgap-Graded Semiconductor Nanowires. *Nano Lett.* **2014**, *14*, 3153−3159.
(14) Liu, Y.; Zapien, J. A.; Shan, Y. Y.; Geng, C.-Y.; Lee, C. S.; Lee, S.-T. Wavelength-Controlled Lasing in $Zn_xCd_{1-x}S$ Single-Crystal Nanoribbons. *Adv. Mater.* **2005**, *17*, 1372−1377.
(15) Dang, C.; Lee, J.; Breen, C.; Steckel, J. S.; Coe-Sullivan, S.; Nurmikko, A. Red, Green and Blue Lasing Enabled by Single-Exciton Gain in Colloidal Quantum Dot Films. *Nat. Nanotechnol.* **2012**, *7*, 335−339.
(16) Li, J. B.; Meng, C.; Liu, Y.; Wu, X. Q.; Lu, Y. Z.; Ye, Y.; Dai, L.; Tong, L. M.; Liu, X.; Yang, Q. Wavelength Tunable CdSe Nanowire Lasers Based on the Absorption-Emission-Absorption Process. *Adv. Mater.* **2013**, *25*, 833−837.
(17) Liu, Y. K.; Zapien, J. A.; Shan, Y. Y.; Tang, H.; Lee, C. S.; Lee, S.-T. Wavelength-Tunable Lasing in Single-Crystal $CdS_{1-x}Se_x$ Nanoribbons. *Nanotechnology* **2007**, *18*, 365606.
(18) Fu, Y. P.; Zhu, H. M.; Stoumpos, C. C.; Ding, Q.; Wang, J.; Kanatzidis, M. G.; Zhu, X. Y.; Jin, S. Broad Wavelength Tunable Robust Lasing from Single-Crystal Nanowires of Cesium Lead Halide Perovskites ($CsPbX_3$, X = Cl, Br, I). *ACS Nano* **2016**, *10*, 7963−7972.
(19) Pan, A. L.; Zhou, W.; Leong, E. S. P.; Liu, R.; Chin, A. H.; Zou, B. S.; Ning, C. Z. Continuous Alloy-Composition Spatial Grading and Superbroad Wavelength-Tunable Nanowire Lasers on a Single Chip. *Nano Lett.* **2009**, *9*, 784−788.
(20) Lu, J. F.; Xu, C. X.; Li, F. T.; Yang, Z.; Peng, Y. Y.; Li, X. Y.; Que, M. L.; Pan, C. F.; Wang, Z. L. Piezoelectric Effect Tuning on ZnO Microwire Whispering-Gallery Mode Lasing. *ACS Nano* **2018**, *12*, 11899−11906.
(21) Lin, W.-Y.; Chen, C.-Y.; Lu, H.-H.; Chang, C.-H.; Lin, Y.-P.; Lin, H.-C.; Wu, H.-W. 10 m/500 Mbps WDM Visible Light Communication Systems. *Opt. Express* **2012**, *20*, 9919−9924.
(22) Cossu, G.; Khalid, A. M.; Choudhury, P.; Corsini, R.; Ciaramella, E. 3.4 Gbit/s Visible Optical Wireless Transmission Based on RGB LED. *Opt. Express* **2012**, *20*, B501−B506.
(23) Kotani, A.; Witek, M. A.; Osiri, J. K.; Wang, H.; Sinville, R.; Pincas, H.; Barany, F.; Soper, S. A. EndoV/DNA Ligase Mutation Scanning Assay Using Microchip Capillary Electrophoresis and Dual-Color Laser-Induced Fluorescence Detection. *Anal. Methods* **2012**, *4*, 58−64.
(24) Tang, S.-J.; Liu, Z.; Qian, Y.-J.; Shi, K.; Sun, Y.; Wu, C.; Gong, Q.; Xiao, Y.-F. A Tunable Optofluidic Microlaser in a Photostable Conjugated Polymer. *Adv. Mater.* **2018**, *30*, 1804556.

DOI: 10.1021/acsnano.9b05110
ACS Nano 2019, 13, 9965−9972

(25) Rodriguez-Ruiz, I.; Ackermann, T. N.; Munoz-Berbel, X.; Llobera, A. Photonic Lab-on-a-Chip: Integration of Optical Spectroscopy in Microfluidic Systems. *Anal. Chem.* **2016**, *88*, 6630−6637.
(26) Liu, X. F.; Zhang, Q.; Xiong, Q. H.; Sum, T. C. Tailoring the Lasing Modes in Semiconductor Nanowire Cavities Using Intrinsic Self-Absorption. *Nano Lett.* **2013**, *13*, 1080−1085.
(27) Liu, X. F.; Zhang, Q.; Yip, J. N.; Xiong, Q. H.; Sum, T. C. Wavelength Tunable Single Nanowire Lasers Based on Surface Plasmon Polariton Enhanced Burstein-Moss Effect. *Nano Lett.* **2013**, *13*, 5336−5343.
(28) Xing, J.; Liu, X. F.; Zhang, Q.; Ha, S. T.; Yuan, Y. W.; Shen, C.; Sum, T. C.; Xiong, Q. H. Vapor Phase Synthesis of Organometal Halide Perovskite Nanowires for Tunable Room-Temperature Nanolasers. *Nano Lett.* **2015**, *15*, 4571−4577.
(29) Mayer, B.; Rudolph, D.; Schnell, J.; Morkötter, S.; Winnerl, J.; Treu, J.; Müller, K.; Bracher, G.; Abstreiter, G.; Koblmüller, G.; Finley, J. J. Lasing from Individual GaAs-AlGaAs Core-Shell Nanowires Up to Room Temperature. *Nat. Commun.* **2013**, *4*, 2931.
(30) Qian, F.; Li, Y.; Gradečak, S.; Park, H.-G.; Dong, Y. J.; Ding, Y.; Wang, Z. L.; Lieber, C. M. Multi-Quantum-Well Nanowire Heterostructures for Wavelength Controlled Lasers. *Nat. Mater.* **2008**, *7*, 701−706.
(31) Huang, M. H.; Mao, S.; Feick, H.; Yan, H. Q.; Wu, Y. Y.; Kind, H.; Weber, E.; Russo, R.; Yang, P. D. Room-Temperature Ultraviolet Nanowire Nanolasers. *Science* **2001**, *292*, 1897−1899.
(32) Johnson, J. C.; Choi, H.-J.; Knutsen, K. P.; Schaller, R. D.; Yang, P.; Saykally, R. J. Single Gallium Nitride Nanowire Lasers. *Nat. Mater.* **2002**, *1*, 106−110.
(33) Duan, X. F.; Huang, Y.; Agarwal, R.; Lieber, C. M. Single-Nanowire Electrically Driven Lasers. *Nature* **2003**, *421*, 241−245.
(34) Chu, S.; Wang, G. P.; Zhou, W. H.; Lin, Y. Q.; Chernyak, L.; Zhao, J. Z.; Kong, J. Y.; Li, L.; Ren, J. J.; Liu, J. L. Electrically Pumped Waveguide Lasing from ZnO Nanowires. *Nat. Nanotechnol.* **2011**, *6*, 506−510.
(35) Piccione, B.; Cho, C.-H.; van Vugt, L. K.; Agarwal, R. All-Optical Active Switching in Individual Semiconductor Nanowires. *Nat. Nanotechnol.* **2012**, *7*, 640−645.
(36) Yang, Y.; Wang, K.; Liang, H.-W.; Liu, G.-Q.; Feng, M.; Xu, L.; Liu, J.-W.; Wang, J.-L.; Yu, S.-H. A New Generation of Alloyed/Multimetal Chalcogenide Nanowires by Chemical Transformation. *Sci. Adv.* **2015**, *1*, e1500714.
(37) Liu, J. Graphene/ZnO Single-Mode Lasing. *Sci. Bull.* **2018**, *63*, 527−528.
(38) Zong, H.; Yang, Y.; Ma, C.; Feng, X. H.; Wei, T.; Yang, W.; Li, J.; Li, J.; You, L.; Zhang, J.; Li, M.; Pan, C.; Hu, X.; Shen, B. Flexibly and Repeatedly Modulating Lasing Wavelengths in a Single Core-Shell Semiconductor Microrod. *ACS Nano* **2017**, *11*, 5808−5814.
(39) Maslov, A. V.; Ning, C. Z. Reflection of Guided Modes in a Semiconductor Nanowire Laser. *Appl. Phys. Lett.* **2003**, *83*, 1237−1239.
(40) Pauzauskie, P. J.; Sirbuly, D. J.; Yang, P. D. Semiconductor Nanowire Ring Resonator Laser. *Phys. Rev. Lett.* **2006**, *96*, 143903.
(41) Xiao, Y.; Meng, C.; Wu, X. Q.; Tong, L. M. Single Mode Lasing in Coupled Nanowires. *Appl. Phys. Lett.* **2011**, *99*, 023109.
(42) Liu, Z. C.; Yin, L. J.; Ning, H.; Yang, Z. Y.; Tong, L. M.; Ning, C.-Z. Dynamical Color-Controllable Lasing with Extremely Wide Tuning Range from Red to Green in a Single Alloy Nanowire Using Nanoscale Manipulation. *Nano Lett.* **2013**, *13*, 4945−4950.
(43) Gu, F. X.; Yang, Z. Y.; Yu, H. K.; Xu, J. Y.; Wang, P.; Tong, L. M.; Pan, A. L. Spatial Bandgap Engineering along Single Alloy Nanowires. *J. Am. Chem. Soc.* **2011**, *133*, 2037−2039.
(44) Xu, J.; Zhuang, X.; Guo, P.; Zhang, Q.; Huang, W.; Wan, Q.; Hu, W.; Wang, X.; Zhu, X.; Fan, C.; Yang, Z.; Tong, L.; Duan, X.; Pan, A. Wavelength-Converted/Selective Waveguiding Based on Composition-Graded Semiconductor Nanowires. *Nano Lett.* **2012**, *12*, 5003−5007.
(45) Samuel, L.; Brada, Y.; Beserman, R. Fundamental Absorption Edge in Mixed Single Crystals of II-VI Compounds. *Phys. Rev. B: Condens. Matter Mater. Phys.* **1988**, *37*, 4671.
(46) Xu, J.; Zhuang, X.; Guo, P.; Huang, W.; Hu, W.; Zhang, Q.; Wan, Q.; Zhu, X.; Yang, Z.; Tong, L.; Duan, X.; Pan, A. Asymmetric Light Propagation in Composition-Graded Semiconductor Nanowires. *Sci. Rep.* **2012**, *2*, 820.
(47) Lu, Y. Z.; Gu, F. X.; Meng, C.; Yu, H. K.; Ma, Y. G.; Fang, W.; Tong, L. M. Multicolour Laser from a Single Bandgap-Graded CdSSe Alloy Nanoribbon. *Opt. Express* **2013**, *21*, 22314−22319.
(48) Siegman, A. E. *Lasers*; Oxford University Press: Oxford, U.K., 1986.
(49) Spillane, S. M.; Kippenberg, T. J.; Painter, O. J.; Vahala, K. J. Ideality in a Fiber-Taper-Coupled Microresonator System for Application to Cavity Quantum Electrodynamics. *Phys. Rev. Lett.* **2003**, *91*, 043902.
(50) Zhang, X.; Cao, Q. T.; Wang, Z.; Liu, Y. X.; Qiu, C. W.; Yang, L.; Gong, Q.; Xiao, Y. F. Symmetry-breaking-induced Nonlinear Optics at a Microcavity Surface. *Nat. Photonics* **2019**, *13*, 21−24.
(51) Morales, A. M.; Lieber, C. M. A Laser Ablation Method for the Synthesis of Crystalline Semiconductor Nanowires. *Science* **1998**, *279*, 208−211.

DOI: 10.1021/acsnano.9b05110
ACS Nano 2019, 13, 9965−9972